Desalination and Water Treatment
www.deswater.com

doi: 10.5004/dwt.2017.20479

75 (2017) 10–17
May

CFD study on the effect of baffle arrangements on flow patterns in tubular membrane channel

Yuanfa Liu[a,*], Xin Luo[a], Gaohong He[b], Yue Yu[a], Jing Guo[a], Yumei Gong[a], Hong Zhang[a]

[a]*School of Textile and Material Engineering, Dalian Polytechnic University, Dalian, China, Tel. +86-15504947974/+86-411-86323131; email: liuyf@dlpu.edu.cn (Y.F. Liu), Tel. +86-18842690361; email: luoxin474@live.com (X. Luo), Tel. +86-13654910863; email: yuyue@dlpu.edu.cn (Y. Yu), Tel. +86-13704091879; email: 13704091879@163.com (J. Guo), Tel. +86-13591770692; email: ymgong@dlpu.edu.cn (Y.M. Gong), Tel. +86-13591398281; email: zhang_hong1234@sina.com (H. Zhang)*
[b]*School of Chemical Engineering, Dalian University of Technology, Dalian, China, Tel. +86-13898498519; email: hgaohong@dlut.edu.cn (G.H. He)*

Received 12 October 2016; Accepted 30 December 2016

ABSTRACT

A computational fluid dynamics (CFD) study was conducted to simulate turbulent flows in tubular membrane channel with different baffle arrangements, i.e., wall baffle, central baffle and baffle combination (combined use of two types of baffle). It reveals that baffle combination generates a rather more complex flow fields within membrane module than single type of baffle, thereby causing the more intense fluctuations of crossflow velocity or wall shear stress and producing the fairly higher turbulence level of fluid flow. Baffle combination can greatly enhances the eddy mixing action in the inter-baffle regions, resulting in the uniform distribution of particle concentration in the vicinity of membrane surfaces. CFD simulation suggests that baffle combination can achieve better membrane filtration performance than single type of baffle, which was validated by the microfiltration experiment.

Keywords: CFD; Turbulence promoter; Microfiltration; Membrane fouling; Flux enhancement

1. Introduction

Membrane fouling, i.e., deposition of rejected particles on membrane surfaces which leads to the blockage of membrane pores [1] or formation of a cake layer [2], is one of the major reasons accounting for the undesirable decline of permeation rate in microfiltration (MF) processes [3]. Membrane fouling is deemed as one of critical factors limiting the use of membrane systems in many applications. To alleviate the adverse effects of membrane fouling, the simple approach is to improve the hydrodynamics condition on the membrane surface. In practice, turbulent flow was widely applied by utilizing different types of turbulence promoters including baffle [4], static mixer [5], static rod [6], twisted wire-rod [7] and helical screw insert [8,9] during the crossflow MF process. Regardless of their configurations, the use of turbulence promoters can effectively improve the membrane filtration performance owing to the high shear stress on the membrane surface. To clearly understand the intrinsic enhancement mechanism, it is necessary to analyze the flow patterns induced by turbulence promoters within membrane modules.

Computational fluid dynamics (CFD) is a powerful tool to investigate the processes involved with fluid flow or heat and mass transfer without recourse to costly experimental work. CFD can provide a lot of information and interesting solutions for the development of various membrane processes including MF [10–12], ultrafiltration (UF) [13–15], nanofiltration [16,17], reverse osmosis [18,19], pervaporation (PV) [20,21], gas separation [22,23], membrane bioreactor [24,25], membrane distillation [26,27], proton exchange membrane fuel cell [28,29], membrane emulsification [30], membrane contactor [31] and membrane reactor [32]. Hwang and Wu [12] developed a CFD model to simulate the rotating-disk dynamic filter system and numerically investigated the

* Corresponding author.

effects of the rotating-disk structure, including the shape and number of vanes, on the distribution of fluid velocity and shear stress acting on the membrane surface. Monfared et al. [15] applied CFD technique to model the UF process in which permeation of solvent molecules was introduced to system via appropriate sink terms in conservation equations. Saeed et al. [19] carried out a CFD study to investigate the effects of dimensionless filament spacing of feed spacer on flow and concentration patterns on membrane surfaces. Liu et al. [21] developed a CFD approach to model the mass transfer in a PV process for obtaining both velocity distribution and concentration profile in the liquid boundary layer of a slit membrane channel. Coroneo et al. [23] developed a CFD model to reliably predict the separation performances of inorganic membranes modules for gas mixture separation. Zhang et al. [27] employed CFD technique to model and simulate the heat and mass transfer processes in hollow-fiber vacuum membrane distillation (VMD) under laminar flow conditions. Hla et al. [32] developed a two-dimensional (2D), axisymmetric CFD model of a tubular catalytic membrane reactor (CMR) to guide the design and operation of a high-temperature water–gas shift-CMR for the processing of coal-derived syngas.

There is a substantial amount of literature focusing on CFD simulation of turbulence promoter-assisted membrane systems [33–36]. Increasingly, more scientists utilized CFD technique to gain insight into the phenomena taking place within membrane modules, assist the design of processes and improve the membrane filtration performance. As one of the simplest type of turbulence promoters, baffle attracts the comprehensive attention due to the simple configuration (being easily manufactured and installed) and high efficiency. There are two types of baffles, i.e., wall baffle (WB) and central baffle (CB) which are constructed in a torus and disc shape, respectively. It has been extensively proved that the use of baffle can improve effectively the membrane filtration performance. To better understand the hydrodynamic effects for flux enhancement, many researchers carried out CFD simulation of baffled membrane systems [37–42]. Wang et al. [37] revealed that CB generated a relatively higher value of wall shear rate than WB in the regions near the corresponding baffles, indicating that CB could achieve a better membrane filtration performance than WB. Liu et al. [38] found that the presence of an array of baffles in the tubular membrane caused remarkable increase in the average cross-flow velocity and shear stress on the wall, which was beneficial to improve greatly the membrane filtration performance. Ahmed et al. [39] reported that the presence of WB in a tubular membrane channel caused intense fluctuation of local wall velocity and shear stress, which was valuable for the enhancement of membrane performance. Ahmed et al. [40] suggested that the baffle orientation played an important role in the flow patterns within membrane module and the right oriented baffle achieved a better membrane filtration performance than the left oriented one. Jafarkhani et al. [41] studied the effects of flow geometric parameters on turbulent flow in a membrane tube equipped with semi-circular baffles. In their study, the pitch to baffle diameter ratio (L/D) and baffle orientation angle were taken into account. Monfared et al. [42] developed a 2D CFD model to numerically study the effects of baffle arrangements on the flux increment for gelatin–water UF in rectangular channel. In the most of previous publications [37–42], single type of baffle (WB or CB) was utilized alone as turbulence promoter to enhance membrane filtration performance. To the best of our knowledge, however, the CFD study on the effects of baffle arrangements on the flow patterns within the tubular MF membrane channel is still limited.

In this study, CFD simulations of baffled membrane systems with three baffle arrangements, i.e., WB, CB and baffle combination, were conducted using the commercial CFD package FLUENT. The aim of this study is to investigate whether baffle combination can achieve a better membrane filtration performance than single type of baffle (WB or CB). The effects of different baffle arrangements on the flow patterns, behavior and feature were numerically investigated through CFD simulations. The contours of velocity magnitude and stream function, and distributions of wall velocity, wall shear stress, turbulent characteristic and static pressure were examined for three baffle arrangements, respectively.

2. Numerical method

2.1. Model geometry

The simulated flow domain is a baffle-filled tubular channel with inner diameter of 15 mm and length of 200 mm. Three kinds of baffle arrangements, namely, WB, CB and baffle combination (combination of WB with CB, termed as WCB), were employed for CFD simulation, as illustrated in Fig. 1. As to WB case, the inner diameter is 10 mm and outer diameter is 15 mm which corresponds to the tube inner diameter. The diameter of CB is 10 mm. The thickness of all baffles is 1 mm. The distance between the channel inlet and the first baffle is set equal to the baffle spacing (distance between two adjacent baffles), which is 15 mm for all cases. As to WCB case, WB and CB are alternately inserted in the tubular channel. Note that there is another kind of baffle combination (combination of CB with WB, termed as CWB). But it was not

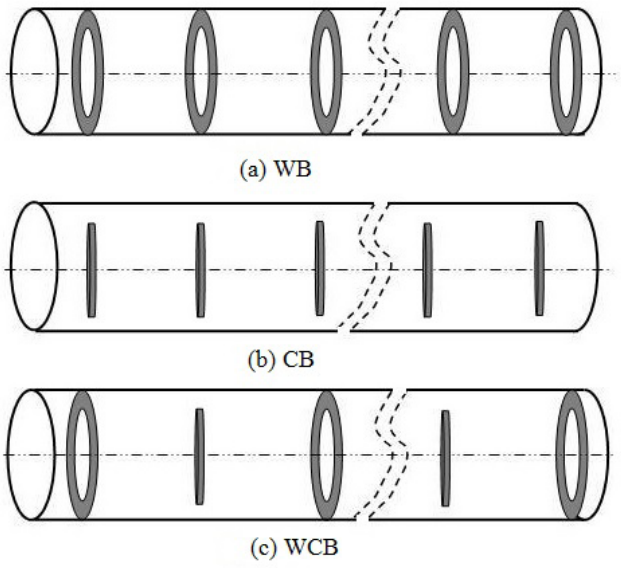

Fig. 1. Schematic diagram of tubular channel with different baffle arrangements.

employed for CFD simulation in this study, because it exhibits almost the similar characteristics of flow field to WCB.

The channel geometry was constructed using the commercial mesh generator GAMBIT. The finer computational grid was employed by utilizing the fixed size function in the vicinity of baffles and channel walls, where higher gradients of velocity and shear stress may exist, as shown in Fig. 2 (taking WCB case as an example). A grid containing about 76,211 cells is adequate to obtain a grid independent solution for the numerical computation.

2.2. Governing equations

The fluid is assumed to be Newtonian and incompressible, and governed by the continuity and Navier–Stokes equations. To facilitate computational solution, the time-averaged method is widely adopted. The time-averaged continuity and Navier–Stokes equations (Reynolds equations) are obtained as follows:

$$\frac{\partial \rho}{\partial t}+\frac{\partial}{\partial x_j}\left(\rho u_i\right)=0 \tag{1}$$

$$\frac{\partial \rho u_i}{\partial t}+\frac{\partial}{\partial x_j}\left(\rho u_i u_j\right)=\frac{\partial}{\partial x_j}\left[\mu\left(\frac{\partial u_i}{\partial x_j}+\frac{\partial u_j}{\partial x_i}\right)-\left(\frac{2}{3}\mu\frac{\partial u_i}{\partial x_i}\right)\right]-\frac{\partial p}{\partial x_i}+\frac{\partial}{\partial x_j}\left\langle-\rho\overline{u_i' u_j'}\right\rangle \tag{2}$$

2.3. Turbulence model

The Re-Normalisation Group (RNG) k–ε model was employed here to simulate the turbulent flow in the baffled channel because it was widely applied for the rotating and swirling flows, which was involved in this study. The enhanced wall treatment available in FLUENT was enabled when the RNG k–ε model was adopted for CFD simulation. In terms of RNG k–ε model, the turbulent kinetic energy k and turbulent dissipation rate ε are determined by the following equations:

$$\frac{\partial(\rho k)}{\partial t}+\frac{\partial(\rho k u_i)}{\partial x_i}=\frac{\partial}{\partial x_j}(\alpha_k \mu_{eff}\frac{\partial k}{\partial x_j})+G_k+G_b-\rho\varepsilon-Y_M+S_k \tag{3}$$

$$\frac{\partial(\rho \varepsilon)}{\partial t}+\frac{\partial(\rho \varepsilon u_i)}{\partial x_i}=\frac{\partial}{\partial x_j}(\alpha_\varepsilon \mu_{eff}\frac{\partial \varepsilon}{\partial x_j})+C_{1\varepsilon}\frac{\varepsilon}{k}(G_k+C_{3\varepsilon}G_b)-C_{2\varepsilon}\rho\frac{\varepsilon^2}{k}-R_\varepsilon+S_\varepsilon \tag{4}$$

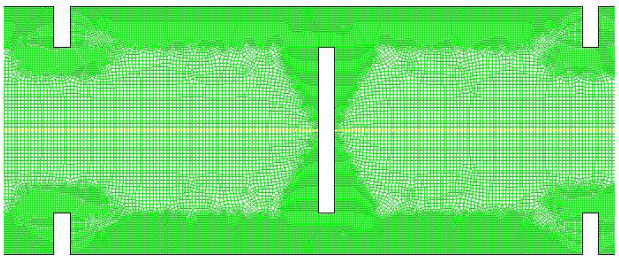

Fig. 2. Computation grid of local partition.

2.4. Mixture model

The mixture model is a simplified multiphase model that is appropriate for the particle-laden flows with low loading where the phases move at different or same velocity. The mixture model can model n phases (fluid or particulate) by solving the volume fraction equations for the secondary phase, and algebraic expressions for the relative velocities. The volume fractions α_q and α_p for a control volume can be equal to any value between 0 and 1, depending on the space occupied by phase q and phase p. The volume fraction equation for secondary phase p is described as follows:

$$\frac{\partial}{\partial t}(\alpha_p\rho_p)+\nabla\cdot(\alpha_p\rho_p\vec{v}_m)=-\nabla\cdot(\alpha_p\rho_p\vec{v}_{dr,p})+\sum_{q=1}^{n}(\dot{m}_{qp}-\dot{m}_{pq}) \tag{5}$$

2.5. Solution method

The commercial CFD package FLUENT (v. 6.3.26) was used to simulate the turbulent flow in the baffled tube. The 2D coordinate system was employed here since the model geometry is axial symmetric about the centerline of tube, which can simplify computational solution. The assumption of non-permeable wall was adopted in this study because it was widely accepted in previously published literature [37–40]. In addition, the no-slip condition on baffles and walls was defined in this study.

The second-order upwind differencing scheme was used to discretize the convective terms. The SIMPLE algorithm was used to resolve the pressure–velocity coupling scheme. The scaled residuals were set to a criterion of at least 10^{-5} for the continuity, momentum and k–ε variables to ensure the solution convergence. In addition, the variation of pressure magnitude at the tube inlet (defined as velocity-inlet boundary condition) and variation of velocity magnitude at the tube outlet (defined as pressure-outlet boundary condition) were monitored simultaneously as an indicator of solution convergence.

3. Results and discussion

In this section, the turbulent flow in the baffled tube was simulated with an inlet velocity of 0.5 m/s (Re = ~7,500 for the empty tube) and outlet pressure of 50 kPa.

3.1. Contours of velocity magnitude

Velocity contours in the baffled tubular channel are shown in Fig. 3. It is well-known that there exists invariably a laminar flow layer in the vicinity of the channel wall for an empty tube whenever the bulk flow is laminar or turbulent. Under the circumstance, the particles in the feed are readily deposited on the membrane surface driven by the filtration flow, resulting in the cake formation and the decay of filtration flux. Obviously, the presence of an array of baffles completely changes the flow fields within membrane module. There is no obvious laminar flow layer in the neighborhood of channel wall for three baffle cases. It is beneficial to alleviate greatly the phenomena of concentration polarization during the membrane filtration process. The baffle arrangement has an important influence on the flow patterns, behavior and

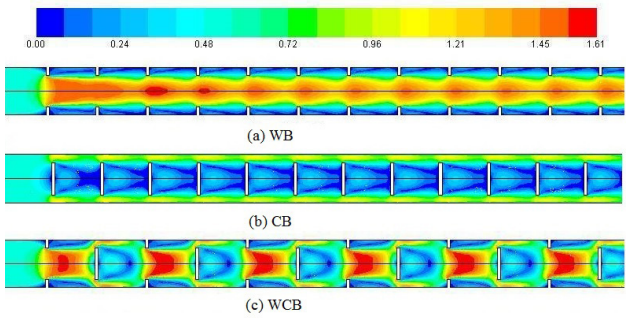

Fig. 3. Effects of baffle arrangement on the velocity contours.

feature in the tubular channel. The distributions of velocity magnitude along the channel are distinctly different for three baffle arrangements. WB generates the higher velocity magnitude at the tube center and the lower velocity magnitude near channel wall. CB produces the relatively higher velocity magnitude on the wall, and lower velocity magnitude at the tube center. For WCB case, the high velocity magnitude alternately appears on the wall or at the tube center. It indicates that baffle combination generates a rather more complex flow fields in tubular channel than single type of baffle (WB or CB). The flow field characteristics in WCB case are distinctly different from that for WB or CB case. Consequently, the distributions of velocity magnitude, wall shear stress and turbulence intensity are different for three baffle arrangements, which will be discussed in the following sections, respectively.

3.2. Distributions of wall velocity and wall shear stress

The distributions of velocity magnitude and shear stress on the channel wall (about 0.1 mm away from the wall) are presented in Fig. 4. It can be observed in Fig. 4(a) that the peak and trough values of velocity magnitude appear periodically along the channel for three baffle cases. The baffle arrangement has a significant influence on the distribution of velocity magnitude. WB generates the peak values of velocity magnitude in the region between baffle intervals and the trough values of velocity magnitude near each WB. CB generates the peak values of velocity magnitude near each CB and the trough values of velocity magnitude in the region between baffle intervals. As to WCB case, the peak values of velocity magnitude appear near each CB and the trough values of velocity magnitude are present near each WB. The fluctuation tendency of wall shear stress is almost similar to that of velocity magnitude for each baffle arrangement, as illustrated in Fig. 4(b). Accordingly, the peak and trough value of wall shear stress periodically appear in the positions where the corresponding values of wall velocity occur. In general, a local peak value of wall shear stress occurs in certain position where the high velocity gradient may exist. It has been reported that peak and trough phenomena can cause a mass transfer difference on the membrane surface.

As shown in Table 1, at the inlet velocity of 0.5 m/s, the peak and trough value of wall velocity is 0.25 and 0.02 m/s for WB case, with the average value of about 0.1 m/s. For CB case, the peak and trough value of wall velocity is 0.71 and

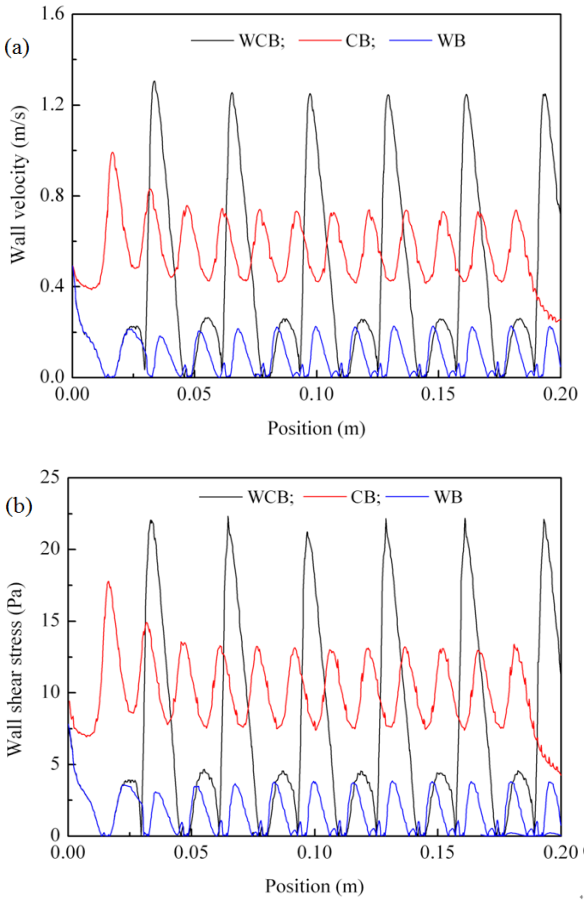

Fig. 4. Effects of baffle arrangement on wall velocity and wall shear stress.

0.42 m/s, with the average value of 0.56 m/s. For WCB case, the peak and trough value of wall velocity is about 1.25 and 0.02 m/s, with the average value of 0.42 m/s, which is much higher than that for WB case but slightly less than that for CB case. Among three baffle cases, WCB produces the biggest difference between peak and trough velocity (1.23 m/s), while WB and CB generate the relatively smaller velocity difference (0.23 m/s for WB case, 0.29 m/s for CB case). It indicates that WCB causes a rather more intense fluctuation of crossflow velocity, making the fluid flow in the baffled tube act as high frequency pulsatile flow, which can enhance significantly local mass transfer on the membrane surface. From this point of view, it can deduce that WCB might achieve better membrane filtration performance than WB or CB.

At the same inlet velocity of 0.5 m/s, WCB produces the greatest peak value of wall shear stress (22.2 Pa), and CB produces the greatest average value of wall shear stress (9.9 Pa) among three baffle cases. It has been widely accepted that high wall shear stress can promote the back transfer of particles away from the membrane surface to the bulk flow due to the action of shear-induced diffusion [43,44]. Although the average value of wall shear stress (6.8 Pa) for WCB case is slightly less than that of CB case (9.9 Pa), it is sufficient enough to improve the membrane filtration performance.

Table 1
Magnitude of wall velocity and wall shear stress for three baffle cases

	Wall velocity (m/s)			Wall shear stress (Pa)		
	Peak value	Trough value	Average value	Peak value	Trough value	Average value
WB	0.25	0.02	0.10	4.4	0.1	1.5
CB	0.71	0.42	0.56	13.1	7.7	9.9
WCB	1.25	0.02	0.42	22.2	0.2	6.8

3.3. Distribution of turbulence characteristics

The distributions of turbulence intensity along the tubular channel with different baffle arrangements are shown in Fig. 5. The turbulence intensity (I) is a direct index of turbulent level of fluid flow or chaos of turbulence, which is defined as the ratio of the random velocity to the time-averaged velocity:

$$I = \frac{u'}{\overline{u}} \times 100\% \tag{6}$$

where u' and $\overline{u}$ is the random velocity and time-averaged velocity, respectively.

The presence of an array of baffles largely increases the local turbulence intensity of fluid flow due to the frequent change in flow direction and the intense fluctuation of velocity fields. Compared with WB or CB, WCB produces the considerably higher turbulence level of fluid flow. The fluid motion remains highly turbulent level in the entire channel, which can disrupt the development of concentration boundary layer to a great extent and minimize the particle deposition on membrane surfaces. From this point of view, it can be concluded that baffle combination can obtain better membrane filtration performance than single type of baffle.

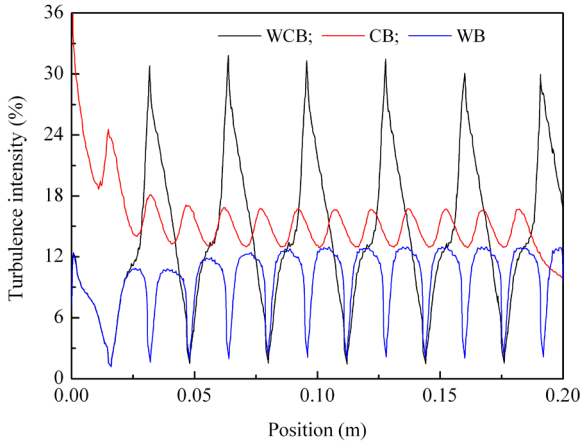

Fig. 5. Effects of baffle arrangement on the turbulence intensity.

3.4. Contours of stream function

The contours of stream function in the tubular channel with different baffle arrangements are shown in Fig. 6. The obvious distortion of local stream lines can be observed in the baffled channel, giving rise to the eddy formation on the downstream side of each baffle. When the fluid flows past each baffle, it creates a space devoid of downstream-flowing fluid on the downstream side of the baffle. Fluid behind the baffle flows into the void creating a swirling of fluid, followed by a short reverse flow of fluid behind the baffle flowing upstream, toward the back of the baffle. Accordingly, the eddy is formed behind each baffle. The baffle arrangement plays an import role in the eddy formation. For WCB case, the eddy magnitude is larger than that for WB case in size, and the eddy strength is stronger than that for CB case, indicating the eddy mixing effect is intensified within membrane module. The eddy mixing can disrupt effectively the development of concentration boundary layer in the inter-baffle regions, thereby promoting the membrane filtration performance. The eddy mixing action facilitates the back transfer of rejected particles away from the membrane surface to the bulk flow, which is responsible for diminishing particles deposition on membrane surfaces. Frankly, eddy formation increases definitely the energy dissipation of turbulent flow, which will be discussed in the following section.

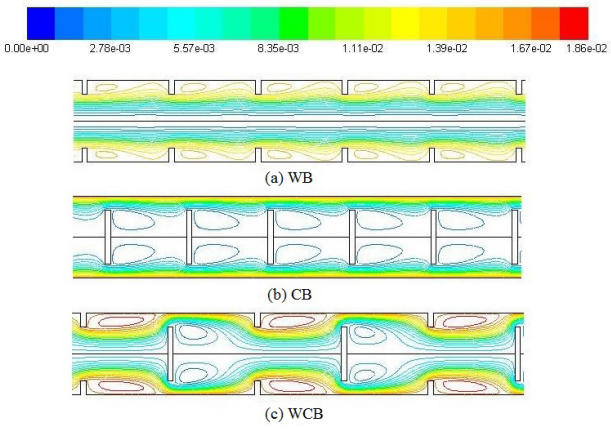

Fig. 6. Effects of baffle arrangement on the stream function.

3.5. Volume fraction of particle phase

To clearly illuminate the action of eddy mixing on the particle deposition on membrane surfaces, the volume fraction of particle phase in the tubular channel with different baffle arrangements was numerically calculated, as shown in Fig. 7. In this section, the simulated fluid is the calcium carbonate suspension. The particle size of calcium carbonate is 5×10^{-6} m. The initial volume fraction of particle phase is 1.84×10^{-4}. In general, the volume fraction of particle phase can directly reflect the particle concentration for the liquid–solid two-phase flow. For an empty tube, there always exists the concentration polarization due to the accumulation of particle phase toward membrane surfaces, as illustrated in

Fig. 7(d). Concentration polarization often leads to the formation of a concentrated boundary layer in the neighborhood of channel wall which may ultimately result in the formation of a cake layer on the membrane surface. It definitely increases the membrane filtration resistance, resulting in the undesired decline of permeate flux with time. The presence of an array of baffles can significantly alleviate the adverse effect of concentration polarization due to the eddy mixing action, because there is no obvious build-up of particle concentration in the vicinity of channel wall for three baffle cases, as illustrated in Figs. 7(a)–(c). For WB case, the particle concentration in the inter-baffle regions is slightly lower than that in the bulk stream due to the fact that eddy formation behind each WB is much close to the channel wall (Fig. 6(a)). For CB case, the particle concentration in the central regions of channel is slightly lower than that in the vicinity of channel wall due to the eddy mixing action, which is consistent with Fig. 6(b). For WCB case, the particle concentration is fairly more uniform in the whole channel, indicating the excellent eddy mixing effect. From this point of view, it can be concluded that WBC might achieve better membrane filtration performance than CB or WB.

3.6. Distribution of static pressure

The distributions of static pressure along the channel with three baffle arrangements are shown in Fig. 8. When the fluid flows past each baffle, it always undergoes an abrupt decline of static pressure, corresponding to the velocity fluctuation and eddy formation. The pressure drop along the channel, which is the pressure difference between the inlet and outlet, is about 3.5, 5.3 and 9.2 kPa for CB, WB and WCB case, respectively. WCB produces the largest pressure drop, indicating the energy cost of membrane module is increased. It probably is due to the frequent change in flow direction and intense velocity fluctuation, increasing the frictional loss of fluid flow. In addition, the enhanced eddy motion is also responsible for the increase of energy cost due to the turbulent energy dissipation.

3.7. MF experiment

In order to validate CFD simulations, the crossflow MF (average pore size of 0.9 μm) of calcium carbonate suspensions (D_{50} = 6.18 μm) was conducted under the same operation conditions with the inlet velocity of 0.5 m/s, transmembrane pressure of 50 kPa and feed concentration of 0.5 g/L. The size of ceramic tubular membrane and geometric parameters of baffles are identical as those depicted in section 2.1. It can be clearly observed from Fig. 9 that WCB achieves better membrane filtration performance than CB or WB under the same operation condition, which is well consistent with the prediction of CFD simulations. It can be well explained by the fact that WCB generates a rather more complex flow fields in tubular channel than WB or CB, thereby causing the more intense fluctuations of crossflow velocity and producing the fairly higher turbulence level of fluid flow. WCB can also enhance the eddy mixing action in the inter-baffle regions, which can effectively disrupt the build-up of particle concentration in the vicinity of membrane surfaces, thereby diminishing the membrane filtration resistance.

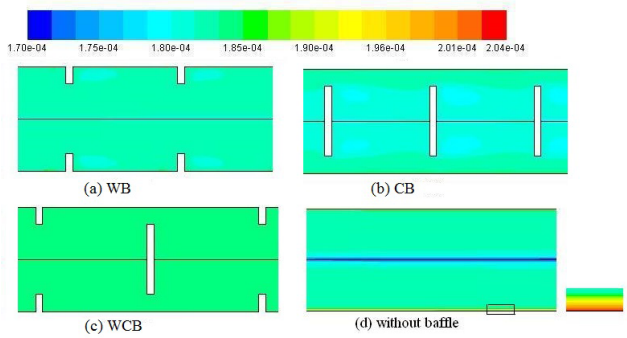

Fig. 7. Effects of baffle arrangement on the volume fraction of particle phase.

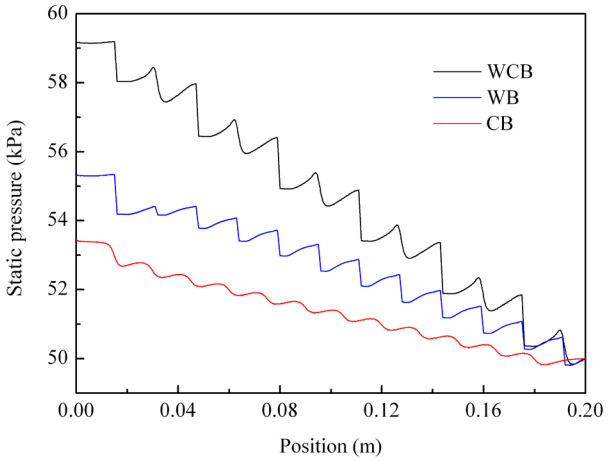

Fig. 8. Distributions of static pressure along the channel with different baffle arrangements.

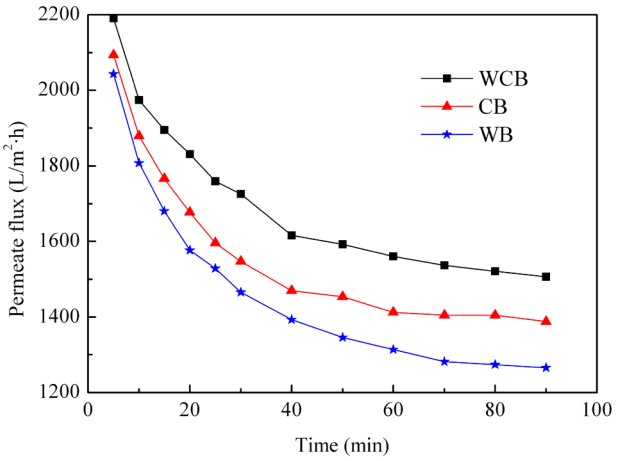

Fig. 9. Effects of baffle arrangement on the membrane permeate flux.

4. Conclusion

The effects of baffle arrangements on the flow patterns, behavior and feature in tubular membrane channel were numerically studied through CFD simulation. Baffle

combination generates a rather more complex flow field than single type of baffle (WB or CB), causes much more intense fluctuations of velocity magnitude and wall shear stress, which is favorable for the membrane filtration process. Baffle combination produces the fairly higher turbulence level of fluid flow within membrane module than single type of baffle, which is beneficial to disrupt the development of concentration boundary layer and prevent particle deposition on the membrane surface. Baffle combination can largely intensify the eddy mixing action in the inter-baffle regions, which can effectively prevent the build-up of particle concentration in the neighborhood of membrane surface. Eddy mixing also tends to facilitate the back transfer of rejected particles away from membrane surfaces to the bulk flow. CFD simulation results indicate that baffle combination can achieve a better membrane filtration performance than single type of baffle, which is validated by the MF experiment. However, as a price, the pressure drop along the tube is increased due to the more frequent changes in flow direction and higher turbulent flow dissipation, indicating the increased energy consumption of membrane module. Hence, the optimization of baffle arrangement involves a trade-off between these competing effects.

References

[1] S. Wang, C. Liu, Q.L. Li, Fouling of microfiltration membranes by organic polymer coagulants and flocculants: controlling factors and mechanisms, Water Res., 45 (2011) 357–365.

[2] Y.F. Liu, G.H. He, B.J. Li, Z.W. Hu, J. Ju, A comparison of cake properties in traditional and turbulence promoter assisted microfiltration of particulate suspensions, Water Res., 46 (2012) 2535–2544.

[3] C.H. Lee, S.H. Lee, P.K. Park, J.H. Kim, K.M. Yeon, Analysis of filtration characteristics in submerged microfiltration for drinking water treatment, Water Res., 42 (2008) 3109–3121.

[4] A.L. Ahmad, A. Mariadas, Baffled microfiltration membrane and its fouling control for feed water of desalination, Desalination, 168 (2004) 223–230.

[5] D.M. Krstic, M.N. Tekic, M.D. Caric, S.D. Milanovic, Kenics static mixer as turbulence promoter in cross-flow microfiltration of skim milk, Sep. Sci. Technol., 38 (2003) 1549–1560.

[6] H.M. Yeh, Y.F. Chen, Modified analysis of permeate flux for ultrafiltration in a solid-rod tubular membrane, J. Membr. Sci., 251 (2005) 255–261.

[7] B.B. Gupta, J.A. Howell, D. Wu, R.W. Field, A helical baffle for cross-flow microfiltration, J. Membr. Sci., 102 (1995) 31–42.

[8] B.J. Bellhouse, G. Costigan, K. Abhinava, A. Merry, The performance of helical screw-thread inserts in tubular membranes, Sep. Purif. Technol., 22–23 (2001) 89–113.

[9] Y. Liu, G. He, M. Tan, F. Nie, B. Li, Artificial neural network model for turbulence promoter-assisted crossflow microfiltration of particulate suspensions, Desalination, 338 (2014) 57–64.

[10] Z. Jalilvand, F.Z. Ashtiani, A. Fouladitajar, H. Rezaei, Computational fluid dynamics modeling and experimental study of continuous and pulsatile flow in flat sheet microfiltration membranes, J. Membr. Sci., 450 (2014) 207–214.

[11] D.C. Choi, S.Y. Jung, Y.J. Won, J.H. Jang, J. Lee, H.R. Chae, K.H. Ahn, S. Lee, P.K. Park, C.H. Lee, Three-dimensional hydraulic modeling of particle deposition on the patterned isopore membrane in crossflow microfiltration, J. Membr. Sci., 492 (2015) 156–163.

[12] K.J. Hwang, S.E. Wu, Disk structure on the performance of a rotating-disk dynamic filter: a case study on microalgae microfiltration, Chem. Eng. Res. Des., 94 (2014) 44–51.

[13] A.L. Ahmad, K.K. Lau, M.Z.A. Bakar, S.R.A. Shukor, Integrated CFD simulation of concentration polarization in narrow membrane channel, Comput. Chem. Eng., 29 (2005) 2087–2095.

[14] K. Darcovich, M.M. Dal-Cin, B. Gros, Membrane mass transport modeling with the periodic boundary condition, Comput. Chem. Eng., 33 (2009) 213–224.

[15] M.A. Monfared, N. Kasiri, A. Salahi, T. Mohammadi, Modeling ultrafiltration of gelatin–water suspension by computational fluid dynamics, Chem. Eng. Res. Des., 90 (2012) 1098–1104.

[16] C. Completo, V. Semiao, V. Geraldes, Efficient CFD-based method for designing cross-flow nanofiltration small devices, J. Membr. Sci., 500 (2016) 190–202.

[17] F. Cortés-Juan, B. Balannec, T. Renouard, CFD-assisted design improvement of a bench-scale nanofiltration cell, Sep. Purif. Technol., 82 (2011) 177–184.

[18] S.S. Bucs, R.V. Linares, J.O. Marston, A.I. Radu, J.S. Vrouwenvelder, C. Picioreanu, Experimental and numerical characterization of the water flow in spacer-filled channels of spiral-wound membranes, Water Res., 87 (2015) 299–310.

[19] A. Saeed, R. Vuthaluru, H.B. Vuthaluru, Investigations into the effects of mass transport and flow dynamics of spacer filled membrane modules using CFD, Chem. Eng. Res. Des., 93 (2014) 79–99.

[20] M. Rezakazemi, M. Shahverdi, S. Shirazian, T. Mohammadi, A. Pak, CFD simulation of water removal from water/ethylene glycol mixtures by pervaporation, Chem. Eng. J., 168 (2011) 60–67.

[21] S.X. Liu, P. Ming, L. Vane, CFD modeling of pervaporative mass transfer in the boundary layer, Chem. Eng. Sci., 59 (2004) 5853–5857.

[22] H. Li, U. Schygulla, J. Hoffmann, P. Niehoff, K. Haas-Santo, R. Dittmeyer, Experimental and modeling study of gas transport through composite ceramic membranes, Chem. Eng. Sci., 108 (2014) 94–102.

[23] M. Coroneo, G. Montante, M.G. Baschetti, A. Paglianti, CFD modelling of inorganic membrane modules for gas mixture separation, Chem. Eng. Sci., 64 (2009) 1085–1094.

[24] X. Liu, W. Yuan, T.D. Waite, G. Leslie, Numerical simulation of bubble induced shear in membrane bioreactors: effects of mixed liquor rheology and membrane configuration, Water Res., 75 (2015) 131–145.

[25] R. Plascencia-Jatomea, F.J. Almazán-Ruiz, J. Gómez, E.P. Rivero, O. Monroy, I. González, Hydrodynamic study of a novel membrane aerated biofilm reactor (MABR): tracer experiments and CFD simulation, Chem. Eng. Sci., 138 (2015) 324–332.

[26] W. Li, H. Wang, B. Li, W. Yue, S. Wang, Novel design of liquid distributors for VMD performance improvement based on cross-flow membrane module, Desalination, 336 (2014) 80–86.

[27] Y. Zhang, Y. Peng, S. Ji, S. Wang, Numerical simulation of 3D hollow-fiber vacuum membrane distillation by computational fluid dynamics, Chem. Eng. Sci., 152 (2016) 172–185.

[28] M.J. Martínez, S. Shimpalee, J.W.V. Zee, Comparing predictions of PEM fuel cell behavior using Maxwell–Stefan and CFD approximation equations, Comput. Chem. Eng., 32 (2008) 2958–2965.

[29] S. Kamarajugadda, S. Mazumder, On the implementation of membrane models in computational fluid dynamics calculations of polymer electrolyte membrane fuel cells, Comput. Chem. Eng., 32 (2008) 1650–1660.

[30] A. Timgren, G. Trägårdh, C. Trägårdh, A model for drop size prediction during cross-flow emulsification, Chem. Eng. Res. Des., 88 (2010) 229–238.

[31] R. Kieffer, C. Charcosset, F. Puel, D. Mangin, Numerical simulation of mass transfer in a liquid–liquid membrane contactor for laminar flow conditions, Comput. Chem. Eng., 32 (2008) 1325–1333.

[32] S.S. Hla, L.D. Morpeth, M.D. Dolan, Modelling and experimental studies of a water–gas shift catalytic membrane reactor, Chem. Eng. J., 276 (2015) 289–302.

[33] Y. Liu, H.E. Gaohong, L. Ding, D. Hong, J.U. Jia, L.I. Baojun, Experimental and CFD studies on the performance of microfiltration enhanced by a turbulence promoter, Chin. J. Chem. Eng., 20 (2012) 617–624.

[34] X. Yang, H. Yu, R. Wang, A.G. Fane, Analysis of the effect of turbulence promoters in hollow fiber membrane distillation

modules by computational fluid dynamic (CFD) simulations, J. Membr. Sci., 415–416 (2012) 758–769.
[35] M. Shakaib, S.M.F. Hasani, M. Mahmood, Study on the effects of spacer geometry in membrane feed channels using three-dimensional computational flow modeling, J. Membr. Sci., 297 (2007) 74–89.
[36] G.A. Fimbres-Weihs, D.E. Wiley, Review of 3D CFD modeling of flow and mass transfer in narrow spacer-filled channels in membrane modules, Chem. Eng. Process., 49 (2010) 759–781.
[37] Y. Wang, J.A. Howell, R.W. Field, D. Wu, Simulation of cross-flow filtration for baffled tubular channels and pulsatile flow, J. Membr. Sci., 95 (1994) 243–258.
[38] Y. Liu, G. He, X. Liu, G. Xiao, B. Li, CFD simulations of turbulent flow in baffle-filled membrane tubes, Sep. Purif. Technol., 67 (2009) 14–20.
[39] S. Ahmed, M.T. Seraji, J. Jahedi, M.A. Hashib, CFD simulation of turbulence promoters in a tubular membrane channel, Desalination, 276 (2011) 191–198.
[40] S. Ahmed, M.T. Seraji, J. Jahedi, M.A. Hashib, Application of CFD for simulation of a baffled tubular membrane, Chem. Eng. Res. Des., 90 (2012) 600–608.
[41] M. Jafarkhani, M.K. Moraveji, R. Davarnejad, F. Moztarzadeh, M. Mozafari, Three-dimensional simulation of turbulent flow in a membrane tube filled with semi-circular baffles, Desalination, 294 (2012) 8–16.
[42] M.A. Monfared, N. Kasiri, A. Salahi, T. Mohammadi, CFD simulation of baffles arrangement for gelatin-water ultrafiltration in rectangular channel, Desalination, 284 (2011) 288–296.
[43] P. Pospisil, R.J. Wakeman, I.O.A. Hodgson, P. Mikulasek, Shear stress-based modelling of steady state permeate flux in microfiltration enhanced by two-phase flows, Chem. Eng. J., 97 (2004) 257–263.
[44] G. Ducom, F.P. Puech, C. Cabassud, Air sparging with flat sheet nanofiltration: a link between wall shear stresses and flux enhancement, Desalination, 145 (2002) 97–102.